Xiaofang Shi and Lizhong Chang*

Equiaxed Solidification of 430 Ferritic Stainless Steel Nucleating on Core-Containing Ti

https://doi.org/10.1515/htmp-2017-0173
Received November 24, 2017; accepted February 12, 2018

Abstract: The solidification structure of ferritic stainless steel can be refined by controlling the contents of Ti, O, and N in the liquid steel through the thermodynamic analysis and high-temperature experiment. It is found by the scanning electron microscopy technology, in which the composite core of Ti nitride-enwrapping Ti oxide can be formed in the solidification front, which promotes the nucleation of δ iron and refines the solidification structure. Meanwhile, the structure analysis of the composite core by the transmission electron microscope technology proves that the Ti oxide that exists in the centre of the composite core is Ti_2O_3 and the Ti nitride that exists in the outer layer of the composite core is TiN.

Keywords: ferritic stainless steel, solidification, thermodynamic, TiN, Ti_2O_3

Introduction

Ferritic stainless steel is a type of nickel-free chromium alloyed steel and plays an increasingly important role in the stainless steel industry. However, certain key technical problems, which restrict the further development of ferritic stainless steel, emerge in the actual production. One of the most important problems is the ridging defect which is related to the solidification structure of stainless steel billets. The solidification structure of the ferritic stainless steel must be refined to obtain a good surface quality and eliminate ridging defect [1–4].

In order to refine the solidification structure, some methods have been employed, such as electromagnetic stirring, low superheat casting etc. However, these methods have not yielded successful results for high-purity ferritic stainless steel. As a heterogeneous nucleation core of δ iron, titanium nitride (TiN) has been extensively investigated in the laboratory since the 1970s. Villafuerte et al. found that the solidification structure of the ferritic stainless steel is mainly the coarse columnar grains when no Ti exists in the steel and that the fine equiaxed grains were obtained when suitable Ti is added to the steel [5–13]. Villafuerte found that the δ iron can nucleate on the surface of TiN with the development of the detection technique, proving that TiN has a good lattice coherence with δ iron and can act as a strong heterogeneous nucleation of the ferritic stainless steel [14]. However, in the actual steelmaking process, TiN may grow into inclusions and even cause TiN aggregation and nozzle clogging [15]. To solve this problem, Columbia Steel in South Africa and Baosteel proposed that the concentration product between Ti and N is less than or equal to 35×10^{-4} based on the factory practice.

If TiN, which served as the heterogeneous cores of δ iron, is used in actual production, the adding amount of Ti must be controlled at a lower level in order to avoid the formation of large TiN inclusions. But the lower Ti content will affect the refining effect of solidification structure. Therefore, how to refine solidification structures with lower Ti content becomes the key to this technology.

Heintze found that TiN grows on the surface of aluminium or Ti oxides in welding experiments [16]. Eijk discovered that TiN also grows on the surface of Mn–Ti–O inclusions [17]. Park et al. found that TiN grows on the surface of MnS when studying the effect of Al on the non-metallic inclusions in Mn–Si-Ti–Mg deoxidized steel and highlighted that MnS and TiN are the face-centred cubic structure, and the disregistry between these structures is 19 % [18]. O. Hiroki proposed that MgO and TiN serve as the heterogeneous nucleation core of δ iron and investigated the effect of Mg or Si deoxidation on the precipitation of TiN in Fe,1.5% Mn,0.05(0.15)%C and 0.1%Ti [19–21]. Takashi found that TiN grows cooperatively with TiOx in his study of the solidification structure refinement of the stainless steel billet adopting core-containing Ti [22]. Kimura et al. and Kim et al. found that the equiaxed solidification was promoted by adding Mg and Ti which affected the amount of TiN as a nucleation agent of δiron [23, 24].

***Corresponding author: Lizhong Chang,** School of Metallurgy Engineering, Anhui University of Technology, Maanshan, China, E-mail: clz1997@163.com
Xiaofang Shi, School of Metallurgy Engineering, Anhui University of Technology, Maanshan, China, E-mail: shixiaofang602@163.com

The above literatures show that TiN is nucleated on the interface of oxide when the fine oxides in the liquid steel can be formed. The ability of TiN-coating oxide to promote δ iron nucleation is comparable to that of pure TiN, because the outer layer of the core is TiN. If TiN is nucleated on the interface of oxides which exist in the molten steel already, the nucleation resistance is considerably lowered than that of pure TiN and the Ti content in the molten steel for TiN nucleation will also decrease significantly. Therefore, using the composite core to refine solidification structure is an effective method for reducing the Ti content.

In this paper, the author found that the composite core of TiN-enwrapping Ti_2O_3 can be formed in the solidification front by controlling the contents of Ti, O, and N in the liquid steel, which serves as the nucleation core of δiron; thus, the solidification structure can be effectively refined.

Thermodynamic analysis of the formation of Ti_2O_3 and TiN composite core

Ti_2O_3 formation is first desirable in refining the δ iron, and TiN then precipitates at the Ti_2O_3 surface. That is, the formation of Ti_2O_3 precedes that of TiN. Given that [O] and [N] exist in the liquid steel simultaneously, they compete with each other to react with Ti. The Gibbs free energy of the formation of Ti_2O_3 must be less than that of TiN to make Ti_2O_3 preferentially formed over TiN.

The thermodynamic formulas of the TiN formation in the 430 stainless steel are expressed in eqs. (1)–(3) [25].

$$[Ti] + [N] = TiN_{(S)} \tag{1}$$

$$\Delta G^{\theta}_{TiN} = -379000 + 149T\,\mathrm{J/mol} \tag{2}$$

$$\begin{aligned}\Delta G_{TiN} &= \Delta G^{\theta}_{TiN} + RT\ln\frac{a_{TiN}}{a_{Ti}.a_N}\\ &= \Delta G^{\theta}_{TiN} + RT\ln\frac{a_{TiN}}{[\%Ti]\cdot f_{Ti}\cdot[\%N]\cdot f_N}\end{aligned} \tag{3}$$

where a_{TiN} is the activity of TiN, defined as unity; [%Ti] and [%N] are the concentration expressed as mass% of components [Ti] and [N]; f_{Ti} and f_N are the activity coefficients of Ti and N, respectively.

The thermodynamic formulas of Ti_2O_3 formation in the 430 stainless steel are expressed in eqs. (4)–(6) [26].

$$2[Ti] + 3[O] = Ti_2O_{3(s)} \tag{4}$$

$$\Delta G^{\theta}_{Ti_2O_3} = -2.303RTLgK_{Ti_2O_3} = -845928 + 248.6T\,\mathrm{J\cdot mol^{-1}} \tag{5}$$

$$\begin{aligned}\Delta G_{Ti_2O_3} &= \Delta G^{\theta}_{Ti_2O_3} + 2.303RTLg\frac{a_{Ti_2O_3}}{a_{Ti}^2 a_O^3}\\ &= \Delta G^{\theta}_{Ti_2O_3} + 2.303RTLg\frac{a_{Ti_2O_3}}{f_{Ti}^2\cdot f_O^3\cdot[\%Ti]^2\cdot[\%O]^3}\end{aligned} \tag{6}$$

where $a_{Ti_2O_3}$ is the activity of Ti_2O_3, defined as unity; [%Ti] and [%O] are the concentration expressed as mass% of components [Ti] and [O]; and $f_{[Ti]}$ and $f_{[O]}$ are the activity coefficients of Ti and O, respectively.

Figure 1 is the Gibbs free energy of the reaction between N, O, and Ti at 1,767 K which is liquidus of the 430 stainless steel according to eqs. (1)–(6).

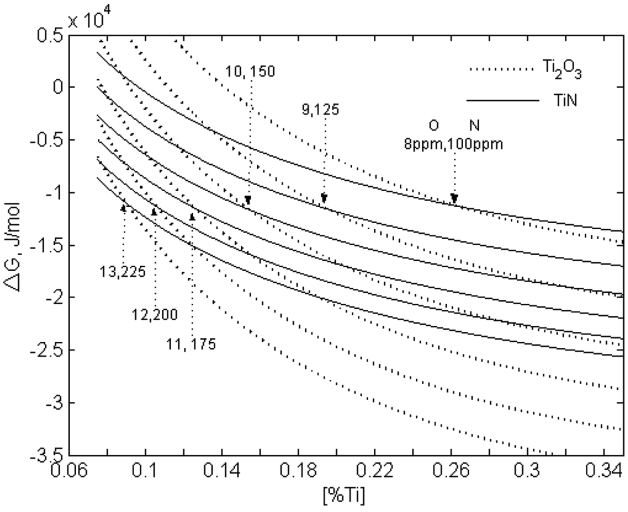

Figure 1: Gibbs free energy of the reaction between nitrogen, oxygen, and titanium.

Figure 1 shows when the [Ti] content is 0.1%–0.2%, [N] content is 0.01%–0.015%, and [O] is 0.001%–0.0022%,$\Delta G_{Ti_2O_3}$ and ΔG_{TiN} are less than zero, and $\Delta G_{Ti_2O_3}$ is less than ΔG_{TiN},which indicates that Ti_2O_3 precipitation precedes that of TiN. ΔG_{Ti2O3} gradually increases with the decrease of [O] and [Ti] contents because of the formation of Ti_2O_3. When the change curves of ΔG_{Ti2O3} and ΔG_{TiN} intersect, TiN begins to form and Ti_2O_3 formation gradually stops.

According to the above analysis, the thermodynamic condition of TiN-enwrapping Ti_2O_3 is reached when the [Ti] content is 0.1%–0.2%, the [N] content is 0.01%–0.015%, and [O] is 0.001%–0.0022%.

Experimental

The experiment was divided into two parts. The influence of Ti and O content on the solidified structure was investigated under the condition that the N content remains mostly unchanged.

Experiments for the different Ti contents

The vacuum induction furnace was used in the experiment, and the technical parameters were as follows: a 10-kg ingot can be melted. The extreme pressure was 6.6×10^{-3} Pa, rated temperature was 1,973 K, and frequency was 4,000 HZ. The vacuum induction furnace was composed of furnace body, feeding chamber, vacuum chamber, and power supply cabinet. The advantage of this furnace was the capability to smelting, pouring, feeding, temperature measuring, and sampling under vacuum conditions. The temperature and the dissolved O content in the molten steel were tested through temperature measuring and O analysis device.

The experimental procedures were as follows.

Vacuum melting. Industrial pure iron and metallic chromium were initially placed in the crucible and then the vacuum pump started up. When the pressure decreased to 800 Pa, the induction furnace began to heating. Metallic silicon and manganese were added to liquid steel for deoxidation and alloying, and the sponge Ti was added to the molten steel after 2 min. When the temperature was 1,853 K, the molten steel was cast into the ingots.

Components analysis. The content of C, Si, Mn, Cr, Al, and Ti was analysed through the spark spectrometric analysis. The samples with a diameter of 5 mm and length of 50 mm were taken from the ingot, and total oxygen (T.O) and total nitrogen (T.N) concentration in the steel were determined by oxygen and nitrogen analyser (Model: ONH-2000).

Macrostructure observation. The finished ingots were longitudinally split in the middle. A mixture of nitric and hydrochloric acids was used after grinding and polishing to erode the surface of the steel.

Scanning electron microscope (SEM) observation. A 15 mm × 15 mm × 15 mm SEM sample was taken from the middle of ingot, and then observed after grinding, polishing, and eroding.

Transmission electron microscope (TEM) observation. "Thin film sample preparation" were available for preparing the TEM sample. First, a thin slice of 8 mm length, 8 mm width, and 0.35 mm thick was taken by a wire-cutting machine and then is polished to 25 μm. Second, a thin film sample with 3 mm diameter and 20 nm thick was obtained through the precision iron-milling system treatment. Finally, The JEM-2100 made in Japan JOF Company was used to observe the morphology of precipitate and analyse the crystal structure of precipitates.

Measurement method of equiaxed grain ratio and size. The solidification structure of ingots was measured by the proportion of equiaxed grains and the size of the grains. In this study, a grain was defined as columnar when the ratio of long to short axis was greater than 2; otherwise, it was an equiaxed grain. The MiVnt software was used to calculate the area of equiaxed (S_E) and columnar grains (S_C); then, S_E and S_C were used to calculate the ratio of equiaxed grain (S) according to eq. (7) [27, 28].

$$S = S_E/(S_E + S_C) \times 100\% \tag{7}$$

According to eq. (8), the average diameter of equiaxed grain could be calculated.

$$\bar{d}_g = \sqrt{\frac{4 \cdot S_E}{n \cdot \pi}} \tag{8}$$

where $\bar{d}_g$ is the average diameter of equiaxed grain; n is the number of equiaxed grains.

Experiments for the different dissolved oxygen contents

Two ingots with different dissolved oxygen content had been made. The experimental equipment was the same as before The experimental process was as follows.

(1) Industrial pure iron and metallic chromium were initially placed in the crucible, and heat began when the pressure reached 73 Pa. Metallic silicon and manganese were added to liquid steel for deoxidation and alloying. The dissolved O was detected, and the sponge Ti was added to liquid steel when the dissolved O was 0.0009 %. When the temperature was 1,842 K, the molten steel was cast into ingots.

(2) Industrial pure iron and metallic chromium were initially placed in the crucible, and heat began when the pressure reached 8,000 Pa. Metallic silicon and manganese were added to the liquid steel for deoxidation and alloying. The dissolved O was detected, and the sponge Ti was added to liquid steel when the dissolved O was 0.0018 %. When the temperature was 1,842 K, the molten steel was cast into ingots.

(3) The component analysis, macrostructure observation, SEM observation, TEM observation, and measurement method of equiaxed grain ratio and size were the same as before.

Change of solidification structure under different conditions

Effect of Ti content on solidification structure

The chemical composition of steel containing the different Ti contents is listed in Table 1. The ferritic stainless steel Nos. 1, 2, 3, and 4 contained Cr, Mn, Si, and Ti. In addition to the change of Ti content, the other compositions were similar. The yield of Ti was between 65 % and 75 % after vacuum induction melting.

Table 1: Chemical composition of steel (%).

Sample	Cr	Mn	Si	T.O	T.N	Ti
No. 1	17.5	0.48	0.85	0.0069	0.011	0.032
No. 2	17.9	0.5	0.66	0.0079	0.0100	0.1
No. 3	18.23	0.43	0.62	0.0072	0.0094	0.14
No. 4	17.84	0.5	0.91	0.0076	0.0095	0.27

The steel macrostructure was shown in Figure 2, in which the inside of the red border indicated an equiaxed grain region and the outside indicated columnar grain region.

According to Formula (7), the equiaxed grain ratio could be calculated, as listed in Table 2.

In Figure 2 and Table 2, the equiaxed grain ratio is only 9.52 % when the Ti content in the steel is 0.032 %. The equiaxed grain ratio increases first and then decreases with the increase of Ti content from 0.032 % to 0.27 %. When the Ti content in the steel is 0.14 %, the equiaxed grain ratio reaches a maximum value of 48.99 %. However, the equiaxed grain ratio decreases to 37.45 % when the Ti content in the steel is 0.27 %. The addition of excessive Ti may lead to precipitation of TiN in molten steel which reduce the precipitation of TiN during solidification and affect the nucleation effect of TiN. Therefore, Ti content in the steel should be controlled at a reasonable range to refine the solidification structure.

Table 2: Change of equiaxed grain ratio with the change of Ti content.

Titanium (%)	0.032	0.1	0.14	0.27
Equiaxed grain ratio (%)	9.52	31.41	48.99	37.45

Effect of dissolved O content on solidification structure

The chemical composition of steel Nos. 5 and 6 containing the dissolved O content is displayed in Table 3.

In Table 3, the content of dissolved O in the two steels was different before adding Ti, and the remaining components were close to each other, where the concentration product between Ti and N was approximately 1.4×10^{-4}.

The steel macrostructure with the different dissolved O is illustrated in Figure 3.

In Figure 3, the centre of the two ingots is full of the equiaxed grains in addition to a few columnar grains at the edges. By calculating the ratio, number, and size of equiaxed grain, their equiaxed grain ratio is higher than 60 %, and the solidification structure of No. 5 is finer than that of No. 6. The number of equiaxed grains in steel Nos. 5 and 6 is nearly 2,600 and 595, respectively, and the grain average diameter is 1.87 mm and 3.93 mm, respectively. The analysis of the solidification structure indicates that the dissolved O content in the steel has an important effect on

Figure 2: Solidification structure of steel containing the different Ti contents.

Table 3: Chemical composition of steel (%).

Sample	Cr	Si	Mn	C	Dissolved O	TO	TN	Ti
No. 5	18.30	0.58	0.38	0.0032	0.00092	0.0073	0.0093	0.14
No. 6	18.08	0.38	0.36	0.0052	0.00181	0.0130	0.0120	0.12

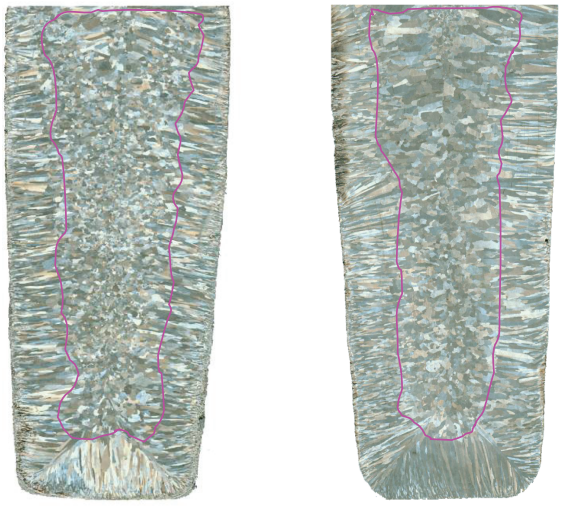

(a) 0.00092% dissolved O (b) 0.00181% dissolved O

Figure 3: Solidification structure of steel with the different dissolved O.

the solidification structure and should be controlled at a reasonable range to refine the solidification structure.

Characteristics of composite core-containing Ti

Morphology of composite core-containing Ti

The composite cores were exposed by eroding the steel, and their morphologies were observed by SEM, as shown in Figure 4. In Figure 4, the morphology of Ti oxide is polygonal and that of Ti nitride is cubic.

Figure 4 displays only the outer surface of the core. The sample is polished with metallographic sandpaper first to observe the inner structure of the core, and the two-dimensional morphology of core is observed by SEM as illustrated in Figure 5. In Figure 5, the cores are composed of two phases, and the dark part at the centre of the core is Ti oxide; the pale part in the outer part of the core is Ti nitride.

Crystal structure of composite core-containing Ti

The SEM observation preliminary proves that the outer part of the composite core is Ti nitride and the inner part is Ti oxide. However, using the results observed by SEM to confirm the crystal structure of the composite core of Ti nitride-enwrapping Ti oxide is inadequate. The crystal structure of the composite core (such as the structure of Ti_2O_3 or Ti_3O_5 at the centre of the core) cannot be determined because the energy spectrum cannot accurately measure the content of low atomic number elements, such as O and N.

To observe the morphology of precipitates and analyse crystal structure, the eight samples were scanned by JEM-2100, and the distribution of the different elements in the precipitate is illustrated in Figure 6. In Figure 6, Ti is distributed evenly in the core, O is mainly concentrated

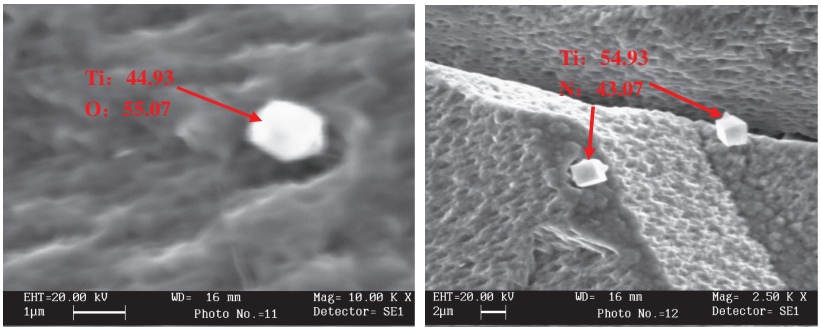

(a) Ti oxide (b) Ti nitride

Figure 4: Morphology of composite core-containing Ti.

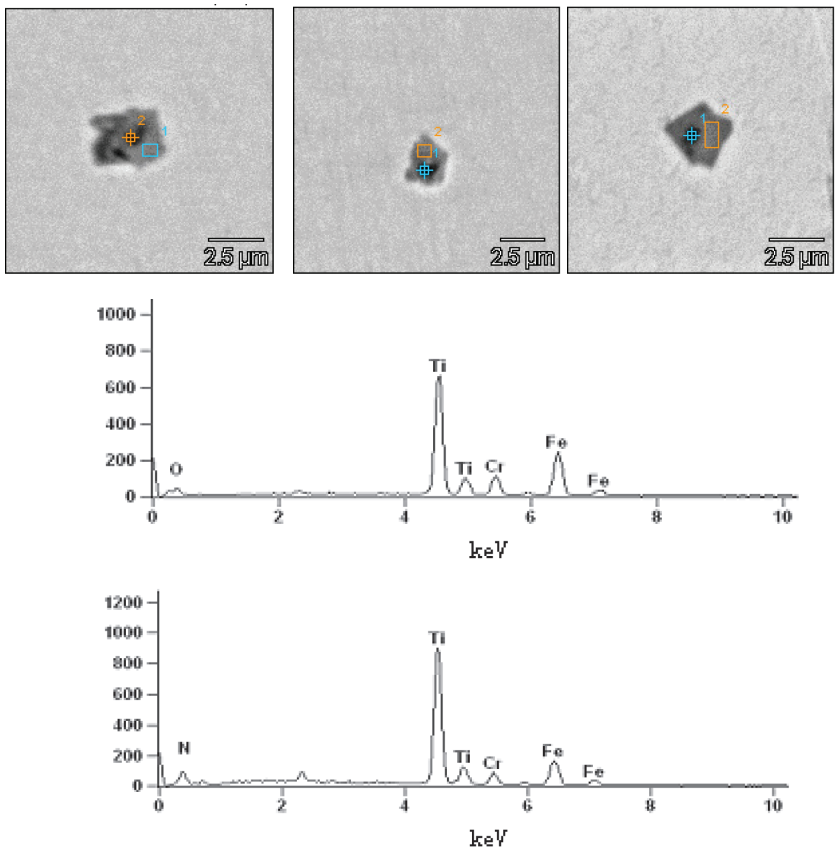

Figure 5: Two-dimensional morphology of composite core and energy spectrum. (a) Energy spectrum of the darker part in the centre of core. (b) Energy spectrum of the pale part in the outer of core.

in the *A* area, and N is mainly concentrated in the *B* area. Carbon is also observed because of the excitation of atoms in high vacuum and therefore does not originate from the precipitate. In Figure 6, the precipitate is a composite core of Ti nitride-enwrapping Ti oxide.

The typical precipitate is selected for structural analysis, and the bright-field image of precipitate is depicted in Figure 7, where the chemical composition in the central black area (*C* area) is mainly O and Ti, and the chemical composition in the lighter area is mainly N and Ti.

The electron diffraction is made in the *C* and *D* areas, and the crystal structure can be obtained by indexing the electron diffraction patterns.

The indexing results are listed in Figure 8, where the crystal parameters in the *C* area coincide with those of Ti_2O_3, and the incident directions of electron beams are [001]. The crystal parameters in the *D* area coincide with those of TiN, and the incident directions of electron beams are $[12\bar{5}]$.

The results of TEM can further prove that the precipitate is a kind of the composite core of TiN-enwrapping Ti_2O_3. In addition, previous literature [29–31] highlighted that the molecular formula of Ti oxide is Ti_2O_3 in pure liquid iron when the Ti content is more than 0.25 %, and the molecular formula of Ti oxide is Ti_3O_5 when the Ti content is less than 0.25 %. However, the author found that Ti_2O_3 will form by thermodynamic calculation in the 430 ferritic stainless steel as long as the Ti content is greater than 0.09 %, which is obviously less than that in the literatures. Therefore, the morphology, electron diffraction patterns, and the indexing results of the composite core-containing 0.1 % and 0.27 % Ti are observed and analysed to prove the accuracy of the thermodynamic calculations, as illustrated in Figure 9.

The indexing results in Figure 9 indicate that the molecular formula of Ti oxide is all Ti_2O_3 in the centre of the composite core (namely, *E* and *F* areas), and the incident directions of electron beams are $[2\bar{2}01]$ and $[\bar{2}20\bar{1}]$, respectively. Therefore, Ti_2O_3 can exist stably in 430 ferritic stainless steel when the Ti content is between 0.1 % and 0.27 %.

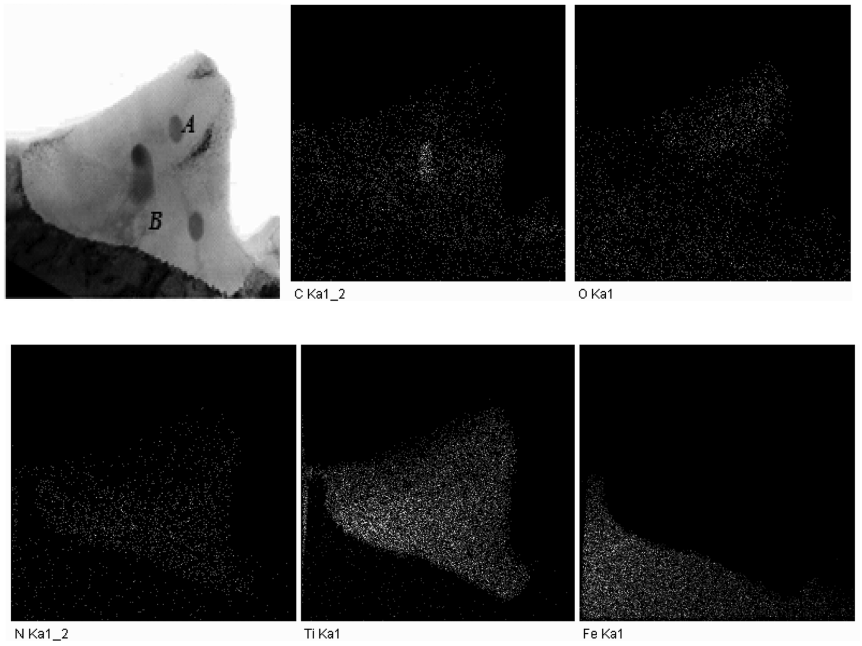

Figure 6: Element distribution in the composite core.

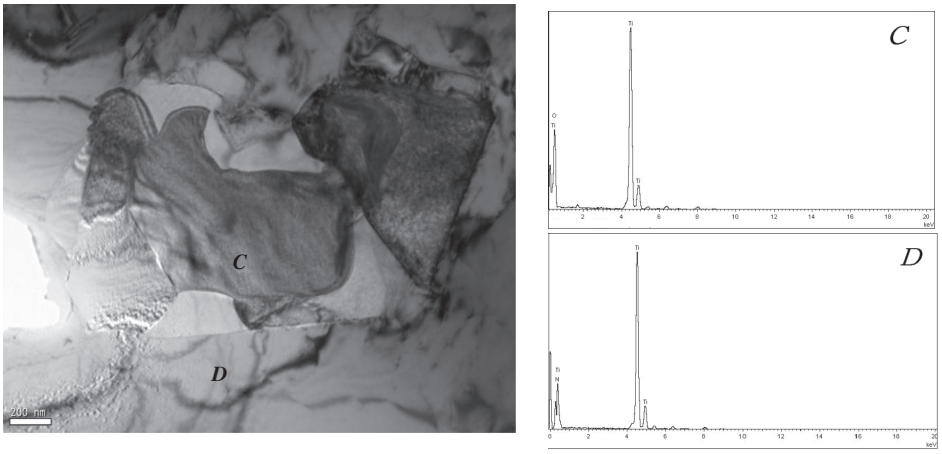

Figure 7: Morphology in the bright-field image of precipitate.

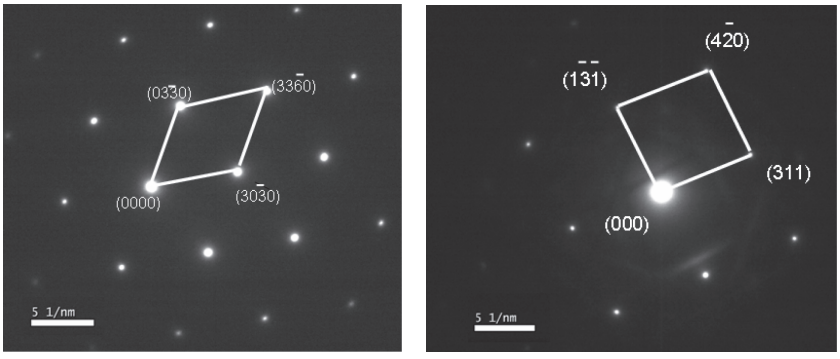

C area D area

Figure 8: Electron diffraction patterns and indexing results of composite core-containing titanium.

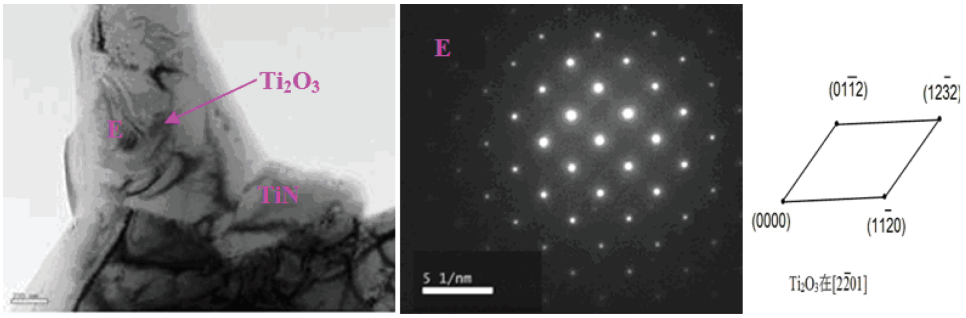

(a) Ti=0.1%

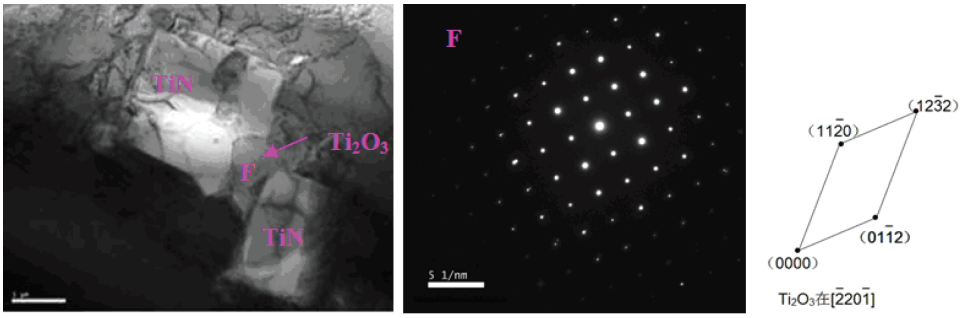

(b) Ti=0.27%

Figure 9: Morphology, electron diffraction patterns, and the indexing results of composite core-containing 0.1% and 0.27% Ti.

Conclusions

This study has proven that the solidification structure of 430 ferritic stainless steel can be refined because of heterogeneous nucleation by controlling the content of Ti, O, and N through a high-temperature experiment. The morphology and the crystal structure of heterogeneous core have been observed by SEM and TEM, and the following results have been obtained.

(1) The solidification structure can be refined by adding proper Ti to 430 ferritic stainless steel and controlling the content of Ti, O, and N. The main reason is the formation of the composite core-containing Ti, which promotes the nucleation of δ iron.

(2) The composite core is made of Ti nitride and Ti oxide by SEM, and Ti oxide is coated with Ti nitride.

(3) Ti_2O_3 can exist stably in the centre of the composite core through the structural analysis of composite core by TEM, which is consistent with the theoretical analysis.

Funding: The work is financially supported by the National Natural Science Foundation of China (Grant No. 51504001, 51574001).

References

[1] K.M. Lee, J. Park, S. Kim, S. Park and M.Y. Huh, Microsc. Microanal., 19 (2013) 17–20.
[2] J. Mola, I. Jung, J. Park, D. Chae and B.C. De Cooman, Metall. Trans., 43 A. (2012). 228–244.
[3] Y. Yazawa, O. Furukimi, Y. Ozaki, Y. Kato and M. Muraki, JP20010334176 [P] (2001).
[4] A. Hunter and M. Ferry, Metall. Mater. Trans., 33 (2002) 1499–1507.
[5] W.J. Poole, A. Mitchell and F. Weinberg, High Temp. Mater. Processes, 16 (1997) 173–182.
[6] T. Koseki, H. Inoue and J. Jpn, Inst. Met., 65 (2001) 644–651.
[7] J.C. Villafuerte, E. Pardo and H.W. Kerr, Metall. Trans., 21 A. (1990). 2009–2019.
[8] V. Villaret, F. Deschaux-Beaume F and C. Bordreuil, J. Mater. Process. Technol., 233 (2016) 115–124.
[9] J.W. Fu, Q.Q. Nie, W.X. Qiu, J.J. Sun, F. Li, Y.C. Wu and J. Mater, Process. Technol., 253 (2018) 43–50.
[10] Y.T. Shan, X.H. Luo, X.Q. Hu and S. Liu, J. Mater. Sci. Technol., 27 (2011) 352–358.
[11] C. Wang, H.Y. Gao, Y.B. Dai, X.M. Ruan, J. Wang and B.D. Sun, Metall. Mater. Trans., 41 (2010) 1616–1620.
[12] H.P. Wang, L.F. Sun, J.J. Shi, C.J. Liu, M.F. Jiang and C. Zhang, Rare Met., 33 (2014) 761–766.
[13] T. Koseki and H. Inoue, J. Jpn. Inst. Met., 65 (2001) 644–651.
[14] J.C. Villafuerte, H.W. Kerr and S.A. David, Mater. Sci. Eng., 194 A. 1995. 187–191.

[15] G. Yang and S. Kenichi, ISIJ Int., 33 (1993) 291–297.
[16] G.N. Heintze and R. McPherson, Weld J. (Miami Fla)., 65 (1986) 71s–82s.
[17] C. Van Der Eijk, J. Walmsley and Ø. Grong, ASM Proc. Int. Conf. Trends Weld. Res., ASM, Phoenix., (2002) 730–735.
[18] S.C. Park, I.H. Jung, K.S. Oh and H.G. Lee, ISIJ Int., 44 (2004) 1016–1023.
[19] O. Hiroki and S. Hideaki, ISIJ Int., 46 (2006) 14–21.
[20] O. Hiroki and S. Hideaki, ISIJ Int., 46 (2006) 480–489.
[21] S. Hideaki, O. Hiroki and M. Shuhei, ISIJ Int., 46 (2006) 840–846.
[22] T. Kawagoe, T. Yamauchi, N. Hiruhama and I. Noguchi, JP19990222037 [P] (1999).
[23] K. Kimura, S. Fukumoto, G.I. Shigesato and A. Takahashi, ISIJ Int., 53 (2013) 2167–2175.
[24] Y.J. Kim, N.R. Oh, Y.H. Oh, Y.T. Cho, W.B. Lee, S.K. Kim and H.U. Hong, Mater. Charact., 132 (2017) 348–353.
[25] J.J. Pak, Y.S. Jeong, I.K. Hong, W.Y. Cha, D.S. Kim and Y.Y. Lee, ISIJ Int., 45 (2005) 1106–1111.
[26] O.J. Jo, J.B. Lee, S.I. Kim, T.I. Chung, W.Y. Kim, J.J. Pak, J.H. Park and D.S. Kim, Int. Symp. Adv. Proc. Metals Mater. Proc. Int. Symp.TMS, San Diego., 2 (2006) 185–198.
[27] W.T. Zhang, Y. Jiang, M.C. Wang, L.N. Zhang and Y.Y. Guo, Journal of Beijing Normal University (Natural Science), 51 (2015) 154–159. (in Chinese).
[28] L.L. ZHOU, C.D. ZHOU, G. LIN, C.Q. WANG, D.W. LIN and H.W. SONG, PTCA(PART: APHYS.TEST.)., 42 (2006) 554–557. (in Chinese).
[29] W.Y. Cha, T. Nagasaka, T. Miki, Y. Sasaki and M. Hino, ISIJ Int., 46 (2006) 996–1005.
[30] W.Y. Cha, T. Miki, Y. Sasaki and M. Hino, ISIJ Int., 46 (2006) 987–995.
[31] L. Liao and R.J. Fruehan, I&SM., 16 (1989) 91–97.